the methyl groups. Although we did not perform the calculation for *cis*-$[Pt(CF_3)_2(NH_3)_2]$, the first two MO's are expected to have significant CF_3 character, since CF_3 substitution does not change the general MO sequence, as calculated for phosphine and ethylene compounds. Therefore, the other possible reason may be due to both C-N and C-F stretching vibrational modes of the same symmetry being excited upon molecular ionization. In this case, frequency comparisons between molecule and ion become meaningless, as pointed out by Eland.[30] The fourth band labelled D,E has about twice the area of the other bands and is thus assigned as due to two almost degenerate MO's. Because TMED has no π-acceptor properties, the platinum d_π orbitals, d_{xz} ($1b_1$) and d_{xy} ($1a_2$), are expected to be close in energy. The fourth band is therefore assigned to these platinum d_π orbitals. The assignments for the other bands are made in a way similar to that for $[PtMe_2(TMED)]$.[12]

(c) Complexes *cis*-$[Pt(CF_3)_2(PEt_3)_2]$ and *cis*-$[Pt(CF_3)_2(AsMe_3)_2]$. The low-IE regions of the spectra for these complexes are similar, as shown in Figure 2b,c. The spectra are less resolved than those for the complexes discussed above, but the spectra were fitted most satisfactorily with six bands. In no case does band A or B show resolved vibrational structure, in contrast to the observations for the COD and TMED complexes. Such splitting may not be expected, since the characteristic ν(PC) and ν(AsC) frequencies are too low to give resolved fine structure.[31] The bands A and B (or bands B and C) are also close in energy and fairly broad, which would make vibrational couplings difficult to resolve.

The spectra give very similar He II/He I intensity ratios (Table I), and ionization energies of all bands shift by a similar amount when compared to the corresponding methylplatinum complexes. Thus, it is again not possible to distinguish between the metal orbitals and the metal-ligand σ MO's on an experimental basis. Therefore, the spectral assignments given in Table I are based on the predictions of the MS-Xα calculations on *cis*-$[Pt(CF_3)_2(PH_3)_2]$ and are similar to those for the corresponding dimethylplatinum(II) complexes.

Pt-CF_3 Bonding and the CF_3 Ligand Effect. From the preceding discussions, at least two features of Pt-CF_3 bonding in these complexes can be summarized as follows: (a) There is considerable C-F antibonding character with significant carbon 2s character in the Pt-CF_3 bonds. In contrast, there is essentially only the carbon 2p lone-pair contribution to the σ-donor orbital of the methyl group in Pt-CH_3 bonding. (b) π interactions between filled d_π orbitals on platinum and σ^* orbitals of the perfluoromethyl group are very weak, as evidenced by the very small fluorine character present in the MO's $1b_1$ and $1a_2$. Since similar platinum 6s character is predicted in both Pt-CF_3 and Pt-CH_3 bonds by MS-Xα calculations, in agreement with their comparable NMR trans influence,[5,6] the observed Pt-C shortening (0.04-0.06 Å)[4,32] in bis(trifluoromethyl)platinum(II) complexes compared to dimethylplatinum(II) complexes could only be explained in terms of the different carbon 2s contributions. In forming a bond with platinum, the perfluoromethyl group will naturally approach closer than the methyl group to the Pt atom because of its greater carbon 2s contribution. This interpretation is in accord with Fenske-Hall calculations on $(CF_3)Mn(CO)_5$ and $(CH_3)Mn(CO)_5$.[11]

From this work, combined with our previous study on the corresponding dimethylplatinum(II) complexes, it can also be noted that the CF_3 substituent, R = CF_3, causes greater σ donation from the ligand L to platinum in the phosphine complex *cis*-$[PtR_2L_2]$ (Figure 4c) and less π back-donating from platinum to the ligand L as in the alkene complex (Figure 4b) compared to their derivatives with R = CH_3. The overall effect still results in more positive charge on platinum, as shown experimentally by the higher ionization energies of the Pt 5d orbitals when R = CF_3. The greater positive charge on platinum will naturally lead to the deactivation of the metal center toward oxidative addition, in agreement with the chemical observations. In addition, the higher ionization energies of the platinum 5d as well as σ orbitals account at least in part for the higher thermal stability of the perfluoromethyl complexes.

Conclusions

The UV photoelectron spectra of the *cis*-bis(trifluoromethyl)platinum(II) complexes can be assigned by comparison with the theoretical predictions based on calculations on the model compounds *cis*-$[Pt(CF_3)_2(C_2H_4)_2]$ and *cis*-$[Pt(CF_3)_2(PH_3)_2]$ and by comparison with the spectra of the corresponding dimethylplatinum(II) complexes. The first two ionization bands with low ionization energies are assigned to the platinum-ligand σ orbitals, followed by the essentially nonbonding platinum 5d orbitals. The nature of the Pt-CF_3 σ bonding can be discussed in terms of MS-Xα results. the CF_3 contribution to the Pt-CF_3 σ bonds arises from the C-F antibonding orbitals with considerable carbon 2s character, rather than pure carbon 2p character.

Acknowledgment. We are grateful to the NSERC for financial support.

(30) Eland, J. H. D. *Photoelectron Spectroscopy*, 2nd ed.; Butterworth & Co. Ltd.: London, 1984; p 138.
(31) Rao, C. N. R. *Chemical Applications of Infrared Spectroscopy*; Academic Press Inc. Ltd.: London, 1963.
(32) Wisner, J. M.; Bartczak, T. J.; Ibers, J. A. *Organometallics* **1986**, *5*, 2044.

Contribution from the Department of Chemistry and Biochemistry, University of California, Los Angeles, California 90024

The Emission Spectrum of Ruthenocene: Calculation of the Excited-State Distortions and the Spacings in the Repetitive Pattern

Gary J. Hollingsworth, Kyeong-Sook Kim Shin, and Jeffrey I. Zink*

Received September 29, 1989

The emission spectrum of crystalline ruthenocene at 10 K contains unusually well-resolved vibronic structure. The crystal spectrum consists of two long progressions in the 333-cm^{-1} metal-ring stretching mode that are separated from each other by 165 cm^{-1}. This separation is not present in the spectrum taken from an isooctane glass. Each of the progressions has the same lifetime but has different polarizations. Each of the peaks of the 333-cm^{-1} progression contains sidebands that are repeated throughout the spectrum. The spectrum is quantitatively calculated and interpreted by using the time-dependent theory of electronic spectroscopy. The repetition is interpreted in terms of beats in the recurrence of overlaps in the time domain. The complete spectrum is accurately calculated by using four displaced normal modes. The major displacement is along the metal-ring bond axis with minor contributions from ring tilting modes.

Introduction

The vibronic structure in the emission spectrum of ruthenocene, $Ru(\eta^5\text{-}C_5H_5)_2$, obtained at low temperature from single crystals contains three interesting features. The most striking feature is a repetitive pattern of clusters of bands consisting of a sharp peak and several weaker sidebands. This pattern is repeated over a

0020-1669/90/1329-2501$02.50/0

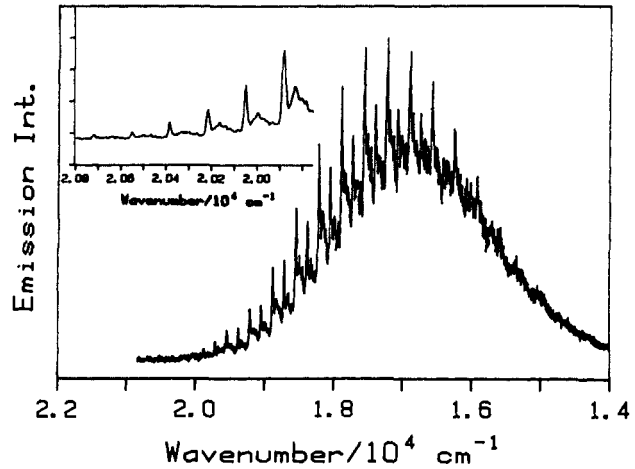

Figure 1. Emission spectrum of $Ru(Cp)_2$ at 10 K. The excitation wavelength is 351.1 nm. The insert shows the high-energy region of the emission spectrum of $Ru(Cp)_2$ containing the origin.

range of greater than 3000 cm^{-1}. Second, the emission spectrum from the crystal is "doubled"; i.e., it contains two almost identical superimposed progressions. Finally, it exhibits a "pincushion" effect, i.e. sharp peaks with widths at half-height of 25 cm^{-1} that are superimposed on a broad "cushion". Two reports of the luminescence spectrum of ruthenocene have recently appeared.[1,2] The emission was assigned to the $^3E_1 \rightarrow {}^1A_1$ transition in D_5. Because the focus of these papers was the assignment of the emitting excited state, the vibronic structure was not analyzed in detail.

The presence of resolved vibronic structure provides the information required to quantitatively determine the distortions along normal vibrational coordinates, which occur when molecules are photoexcited. (More commonly, only broad unstructured bands are obtained from large organometallic compounds in condensed media.) The bond length and bond angle changes can be determined by using the observed vibronic band intensities and either a Franck–Condon analysis or the recent time-dependent theory of electronic spectroscopy.[3-7] The time-dependent theory offers computation ease and new insight into the origins of spectral features. In particular, from the point of view of the time domain, the repetitive pattern in the spectrum can be readily understood and interpreted.

In this paper we report the measurement and analysis of the well-resolved vibronic structure in the crystal emission spectrum of ruthenocene. The spectrum is calculated by using the time-dependent theory of electronic spectroscopy. The repetitive pattern is a result of beats in the overlap of four modes in the time domain. The beats and the spectral consequences are discussed. The intensities of the vibronic bands are calculated, and the distortions that the molecule undergoes upon excitation are calculated and discussed.

Experimental Section

Ruthenocene was obtained commercially from Eastman Kodak and Strem and sublimed before use. The spectra were taken at 10 K with 351.1-nm excitation from the argon ion laser and recorded digitally by using an instrument described previously.[7] The spectra were identical regardless of the excitation wavelength. Emission spectra were also taken at 10 K in an isooctane glass with 351.1-nm excitation.

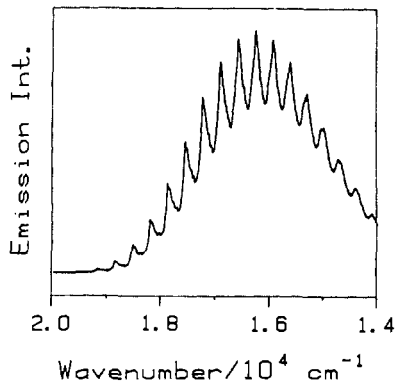

Figure 2. Emission spectrum of $Ru(Cp)_2$ in an isooctane glass at 10 K. The excitation wavelength is 351.1 nm.

Emission decays were measured with an aScope digital memory oscilloscope using 406-nm excitation. System response time was approximately 500 ns, much shorter than the lifetime. Lifetimes were measured by monitoring at 17889, 18056, 18089, 18167, 18211, 18722, and 18889 cm^{-1}. In all cases, the plot of the log of the intensity versus time was linear over at least 3 lifetimes.

Results

The emission spectrum of $Ru(Cp)_2$ at 10 K is shown in Figure 1. The excitation wavelength is 351.1 nm. The spectrum is very broad, covering over 7000 cm^{-1}. The most striking feature is the repeating pattern of sets of sharp peaks. Each set of peaks comprises an intense main peak and several less intense sidebands. The energy separation between the main peak and the sidebands is less than that of any normal mode of the molecule.

The sets of sharp peaks form a progression with a separation of 333 cm^{-1}. This spacing corresponds to the totally symmetric ring–metal stretching mode. There are two such progressions: a main progression and a second less intense progression separated from the first by 165 cm^{-1}. Each progression shows the pattern of sets of peaks. Not only do the progressions overlap, but the peaks within a set also overlap. The effect of so many closely spaced peaks is to give the appearance of a broad underlying emission with the most intense peaks rising above. We have called this resolved line structure on a broad emission the "pincushion".

Because of the overlapping progressions, the large distortions, and, consequently the large number of vibronic bands, it is difficult to ascertain the electronic origin in the spectrum. The high-energy region of the spectrum was carefully examined in order to locate the origin precisely. The insert to Figure 1 shows this region at higher magnification. The first clearly identifiable feature is at 20716 cm^{-1}. It is chosen as the electronic origin of progression I in the work that follows. The peak at 20551 cm^{-1} is chosen as the electronic origin of progression II.

The emission spectrum of ruthenocene in an isooctane glass at 10 K is shown in Figure 2. The excitation wavelength is 351.1 nm. The spectrum contains only one of the progressions that was observed in the crystal spectrum. Although the structure is not as well resolved, the pattern of one intense main peak and less intense side peaks is clearly visible in the glass spectrum, particularly in the region around the origin. The emission is red-shifted by about 1000 cm^{-1} from the emission seen in the crystal.

Polarized emission spectra were taken to determine whether or not the two sets of progressions are polarized differently from each other. The polarized emission spectra of a single crystal at 10 K are shown in Figure 3. The excitation wavelength is 351.1 nm. The spectra were obtained by rotating the polarizer to maximize the intensity of the peak at 18057 cm^{-1} and recording the spectrum. The polarizer was then rotated to minimize the intensity at 18057 cm^{-1}, and the spectrum was recorded again. In the spectrum taken with the polarizer positioned to maximize the intensity at 18057 cm^{-1}, the two progressions show roughly equal intensity. In the spectrum taken with the polarizer positioned to minimize the intensity at 18057 cm^{-1}, the intensities of both progressions are decreased, but the intensity of the second progression is much less than the first. The two progressions have

(1) Wrighton, M. S.; Pdungsap, L.; Morse, D. L. *J. Phys. Chem.* **1975**, *79*, 66.
(2) Crosby, G. A.; Hager, G. D.; Hipps, K. W.; Stone, M. L. *J. Chem. Phys.* **1974**, *28*, 497.
(3) Yersin, H.; Otto, H.; Zink, J. I.; Gliemann, G. *J. Am. Chem. Soc.* **1980**, *102*, 951 and references therein.
(4) Zink, J. I. *Coord. Chem. Rev.* **1985**, *64*, 93.
(5) Zink, J. I.; Tutt, L.; Yang, Y.-Y. *ACS Symp. Ser.* **1986**, *307*, 39.
(6) Preston, D. M.; Shin, K. S.; Hollingsworth, G.; Zink, J. I. *J. Mol. Struct.* **1988**, *173*, 185.
(7) Larson, L. J.; Zink, J. I. *Inorg. Chem.* **1989**, *28*, 3519.

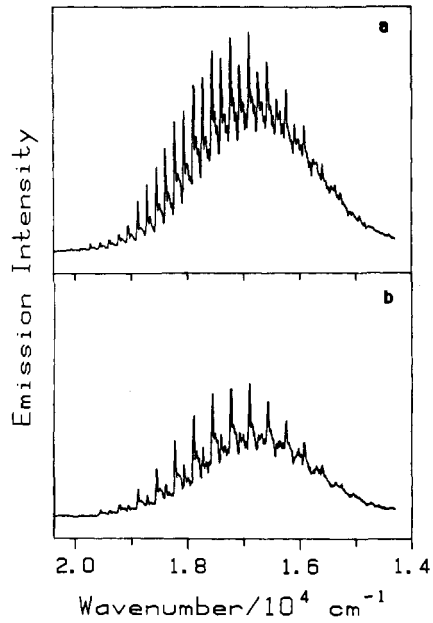

Figure 3. (a) Polarized emission spectrum of $Ru(Cp)_2$ at 10 K taken with intensity maximized at 18057 cm^{-1}. The excitation wavelength is 351.1 nm. (b) Polarized emission spectrum of $Ru(Cp)_2$ at 10 K taken with intensity minimized at 18057 cm^{-1}. The excitation wavelength is 351.1 nm.

significantly different polarizations.

The emission lifetimes of crystals at 12 K in each of the two progressions were measured at a number of frequencies. The frequencies chosen corresponded to the main peaks and to the various sidebands in each of the two progressions. These are 18889 cm^{-1} (the fifth quantum of the main peak in progression II), 18722 cm^{-1} (the sixth quantum of the main peak in progression I), 18211 cm^{-1} (the seventh quantum of the main peak in progression II), 18167 cm^{-1} (the first sideband of the seventh quantum of the main peak in progression II), 18089 cm^{-1} (the second sideband of the seventh quantum of the main peak in progression II), 18056 cm^{-1} (the eigth quantum of the main peak in progression I), and 17899 cm^{-1} (the eighth quantum of the main peak in progression II). In all cases the plots of the log of the intensity versus time were linear and the slopes were the same within experimental error for all of the measurements. The lifetime was 129 ± 2 μs, which is in good agreement with the lifetime of 130 μs previously measured at 20 K.[2]

Discussion

1. The Time-Dependent Theory of Emission Spectroscopy. The time-dependent theory of electronic spectroscopy provides a simple explanation for the repetitive pattern of peaks and sidebands in the emission spectrum. In addition, it provides a quantitative method of calculating the intensities of these features. Because the theory has been discussed in detail previously,[4-7] only a brief discussion of the general aspects will be given here.

The spectra are governed by the motion of a wavepacket on the multidimensional electronic state potential surface. The initial wavepacket, ϕ, is projected onto the ground-state potential energy surface. This surface is, in general, displaced relative to the initial surface, and the wavepacket begins to move, following the path of steepest descent. The displaced wavepacket is not a stationary state of the final surface and evolves according to the time-dependent Schrödinger equation. The emission spectrum is given by[8]

$$I(\omega) = C\omega^3 \int_{-\infty}^{\infty} e^{i\omega t} \langle \phi | \phi(t) \rangle \, dt \qquad (1)$$

where C is a constant and $I(\omega)$ is the intensity in photons per unit volume per unit time at frequency of emitted radiation ω. The quantity $\langle \phi | \phi(t) \rangle$ is the overlap of the initial wavepacket, $\phi(0)$, with the time-dependent wavepacket, $\phi(t)$.

If it is assumed that (a) the normal coordinates are not mixed in the excited state, (b) the transition dipole moment, μ, is constant, and (c) the force constants do not change in the excited state, then the overlap for one specific normal mode (kth) has the simple form for the harmonic potential surfaces

$$\langle \phi_k | \phi_k(t) \rangle = \exp\left[-\frac{\Delta_k^2}{2}(1 - \exp(-i\omega_k t)) - \frac{i\omega_k t}{2} \right] \qquad (2)$$

where ω_k and Δ_k are respectively the vibrational frequency in cm^{-1} and the displacement of the kth normal mode. In the case of many displaced normal modes, the total overlap is

$$\langle \phi | \phi(t) \rangle = \prod_k \langle \phi_k | \phi_k(t) \rangle \exp\left(\frac{-iE_0 t}{\hbar} - \Gamma^2 t^2 \right) \qquad (3)$$

where E_0 is the difference in the electronic energy between the minima of the two surfaces and Γ is a damping factor. Thus, the complete overlap is

$$\langle \phi | \phi(t) \rangle = \exp\left[\sum_k \left[-\frac{\Delta_k^2}{2}(1 - \exp(-i\omega_k t)) - \frac{i\omega_k t}{2} \right] - \frac{iE_0 t}{\hbar} - \Gamma^2 t^2 \right] \qquad (4)$$

2. Analysis of the Repetitive Patterns. The most striking feature in the vibronic structure of the low-temperature emission spectrum of ruthenocene is a repetitive pattern of clusters of bands. The pattern consists of the main peak and three side peaks, which are separated from the main peak by about 47, 65, and 112 cm^{-1}. The first two side peaks are often not well resolved. The separation between the bands within a cluster is less than the energy of any normal mode. A possible explanation for the side peaks could be phonon wings on the main 333-cm^{-1} progression. However, the glass spectrum contains shoulders at about the same positions as the side peaks in the crystal spectrum. If the side peaks were caused by crystal lattice modes, then the shoulders would not be present in the glass spectrum. Thus the structure must arise from molecular normal modes and not from crystal lattice modes.

The time-dependent theoretical point of view provides a simple interpretation of the repetitive pattern. The new insight arises from interpreting the system in the time domain. In the time domain, the overlap as a function of time for a given mode oscillates. The separation between the recurrences is a vibrational period. The total overlap is the product of the overlaps of each of the individual normal modes. Because each contributing mode has a different vibrational period, the product will be modulated and contain "beats". An analogue is found in sound waves. When the difference in frequencies between two sound waves is small compared to the sum of the two, the oscillation is rapid, but its "envelope" undergoes slow periodic variations, known as "beats". For two waves, the beat frequency is the difference between the frequencies of the waves.

The modulation of the overlap in the time domain can be clearly seen from the simplest pedagogical example, that of two modes which are similar in frequency. Figure 4 shows the overlap and spectrum for a molecule having two modes with frequencies of 400 and 500 cm^{-1}. (In this calculation, the displacments are 1.5 for the 400-cm^{-1} mode and 1.0 for the 500-cm^{-1} mode.) At t = 0 the total overlap is 1. The plot of the overlap versus time shows the initial falloff and subsequent recurrences at time τ_1. τ_1 is equal to $2\pi/\omega$, which is between the frequencies of the two modes in consideration. Most importantly, the magnitude of the overlap on successive recurrences rises and falls; i.e. the overlap is modulated. The magnitude is modulated with a beat frequency of 100 cm^{-1}. The modulation occurs with a time τ_2 in the time domain. τ_2 is equal to $2\pi/\Delta\omega$ and is related to the difference in the frequencies. The spectrum in Figure 4 (which is the Fourier transform of the overlap) contains clusters of closely spaced peaks.

(8) (a) Heller, E. J. *J. Chem. Phys.* **1978**, *68*, 2066. (b) Tannor, D. J.; Heller, E. J. *J. Chem. Phys.* **1982**, *77*, 202.

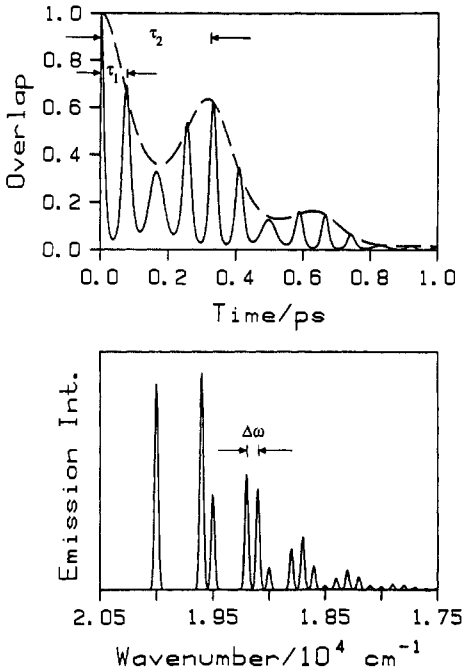

Figure 4. Top: Magnitude of the overlap (—) as a function of time for two modes with equal displacements and Γ less than the difference in frequencies (ω_1 = 400 cm^{-1}, Δ_1 = 1.5; ω_2 = 500 cm^{-1}, Δ_2 = 1.0; Γ = 11 cm^{-1}). The dashed line is a guide to show the modulation. Bottom: Spectrum calculated by taking the Fourier transform of the overlap (E_{00} = 20 000 cm^{-1}).

The separation between the components in a cluster is 100 cm^{-1}.

The damping factor, Γ, can have profound effects on the spectrum. If Γ is much larger than the highest frequency, recurrences in the overlap will be totally damped out and the spectrum will consist of a broad unstructured band. If Γ is larger than the difference in the frequencies, the modulation will be damped out but the first recurrence is still observed. It reaches its maximum at a time between the recurrences of two contributing modes. The corresponding spectrum will show vibronic structure with a frequency between the two frequencies, which is known as the missing mode effect (MIME).[7,9-11] If Γ is less than the difference between the two frequencies, successive recurrences are not damped out and a modulation will appear in the overlap. (The damping factor used to calculate Figure 4 is 11 cm^{-1}.) The Fourier transform of the overlap in the time domain, giving the spectrum in the frequency domain, is a repeating pattern of bands. The separation between the bands is the difference in frequencies.

The time-dependent theoretical analysis shows that the spacings between the components of the repetitive clusters in an emission spectrum can be caused by the beats between normal modes in the time domain. In the case of ruthenocene, the separations between the bands within a cluster are the differences in wavenumbers between the 333-cm^{-1} mode and three other normal modes, the 382-cm^{-1} ring tilt mode, the 400-cm^{-1} ring tilt mode, and the 445-cm^{-1} metal–Cp stretching mode. (The beats in the overlap in the time domain for the full calculation are shown and discussed below.) The differences between the wavenumbers obtained from the bands in the repetitive pattern in the emission spectrum (47, 65, and 112 cm^{-1}) and those taken from the vibrational spectra (49, 67, and 112 cm^{-1}) are in excellent agreement.

Vibronic spacings can also be interpreted by using the standard Franck–Condon analysis. For example, the peak in progression I at 20 050 cm^{-1} (Figure 1) arises from two quanta of the 333-cm^{-1} mode and the lower energy sidebands on this peak arise from the combinations of two quanta of the 333-cm^{-1} mode and one quantum of the 382-cm^{-1} mode, the 400-cm^{-1} mode, or the 445-cm^{-1} mode, respectively.

3. The Doubling of the Repetitive Patterns. Two distinct progressions separated by 165 cm^{-1} occur in the crystal emission spectrum. Both progressions show the pattern of sets of peaks analyzed above. In essence, the spectrum is doubled. This doubling of the spectrum could be caused by emission from multiple excited states or from molecules in different crystal sites or configurations. It could also be the result of two different vibronic origins.

If emission from multiple excited states were the cause of the observed spectrum, it is expected that the lifetimes of the states would be different. Lifetime measurements were made by monitoring the decay at a number of wavelengths. In all of the measurements, the slope of the plot of the log of the intensity versus time was the same. These results do not provide conclusive proof that only one state is emitting. If more than one excited state is involved, the differences in the emission lifetimes could be less than the uncertainty in the measurements (±2 μs). There is no way of predicting how large the differences in lifetimes should be. However, it is unlikely that two different spin–orbit states would have such similar lifetimes.

Doubling of the spectrum could be caused by two different promoting modes whose energy difference is 165 cm^{-1}. This interpretation could also explain the polarization of the emission spectrum (Figure 3), which shows that the two progressions have different polarizations. It is also consistent with the result of thermal modulation spectroscopy.[12]

The result of the spectroscopic studies in glasses are particularly interesting. In isooctane glasses, the doubling disappears. However, Crosby et al.[2] state that the doubling persists in glass. (The type of glass was not stated.) Güdel et al. found that the doubling is present in spectra obtained from durene matrices.[13] It is possible that the doubled spectrum in some glasses results from emission from microcrystals. It is also possible that some glasses favor a molecular conformation in which two promoting modes are active, resulting in the doubled spectra, whereas others favor a conformation from which the doubled spectrum is absent.

Another possibility is that the progressions arise from molecules in two different configurations. An intriguing possibility is that the doubling is caused by emissions from the staggered and eclipsed configurations. The rotational barrier has been estimated to be between 10 and 50 kJ/mol.[14,15] If the intermolecular energies in the glasses or crystals are of greater magnitude than that of the barrier, either configuration may be found. Thus, the presence or absence of the doubling could depend upon the molecule's environment.

The origin of the doubling most likely arises from two different configurations or two different vibronic origins. The experimental facts that there is only one measurable lifetime and that there is only one progression in isooctane glass do not provide a sufficient basis to discriminate between the two explanations.

4. Calculation of the Intensities of Vibronic Bands and the Bond Length Changes in the Excited State. The intensities of vibronic bands in the emission spectrum of ruthenocene are calculated by using a given set of values Δ_k, ω_k, Γ, and E_{00} by use of eqs 1–4. E_{00} and Γ are determined from the emission spectrum. In the following calculations a value of 20 716 cm^{-1} was used for the energy of the electronic origin of progression I. The calculated bands built on this origin correspond to the less intense progression of the experimental spectrum. The origin of the more intense progression is 20 551 cm^{-1} (progression II). The ω_k's are determined from the band spacings in the emission spectrum. These spacings are in agreement with those measured from IR and Raman spectra.[16,17] The presence of two progressions in the

(9) Tutt, L.; Tannor, D.; Heller, E. J.; Zink, J. I. *Inorg. Chem.* **1982**, *21*, 3858.
(10) Tutt, L.; Tannor, D.; Schindler, J.; Heller, E. J.; Zink, J. I. *J. Phys. Chem.* **1983**, *87*, 3017.
(11) Tutt, L.; Zink, J. I. *J. Am. Chem. Soc.* **1986**, *108*, 5830.
(12) Hipps, K. W.; Francis, A. H. *J. Phys. Chem.* **1979**, *83*, 1879.
(13) Güdel, H. Private communication.
(14) Maverick, E.; Dunitz, J. D. *Mol. Phys.* **1987**, *62*, 451.
(15) Cotton, F. A.; Wilkinson, G. *Advanced Inorganic Chemistry*, 4th ed.; Wiley Interscience: New York, 1980; p 100.
(16) Adams, D. M.; Fernando, W. S. *J. Chem. Soc., Dalton Trans.* **1972**, 2507.

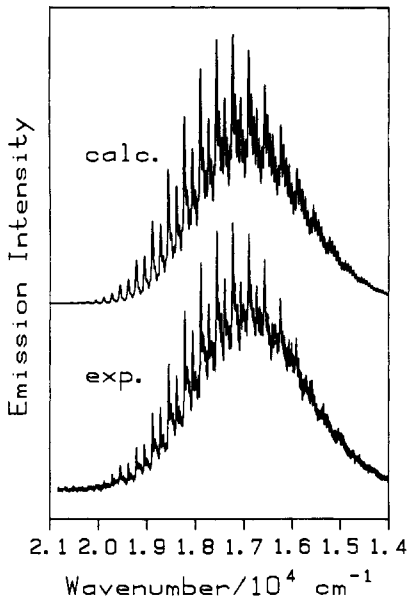

Figure 5. Calculated and experimental emission spectra of $Ru(Cp)_2$.

Table I. Calculated Displacement Δ_k's

k	ω_k, cm^{-1}	assgnt	Δk[a]
		Progression I[b]	
1	333	sym Ru–ring str	4.45
2	382	ring tilt	1.25
3	400	ring tilt	0.83
4	445	asym Ru–ring str	1.20
		Progression II[c]	
1	333	sym Ru–ring str	4.40
2	382	ring tilt	1.10
3	400	ring tilt	0.83
4	445	asym Ru–ring str	1.05

[a] The Δ_k's are displacements of the dimensionless normal coordinates. Progression I is 0.75 times as intense as progression II. [b] E_{00} = 20716 cm^{-1} and Γ = 13 cm^{-1}. [c] E_{00} = 20551 cm^{-1} and Γ = 13 cm^{-1}.

spectrum complicates the fitting procedure. Preliminary determination of the parameters was made by fitting one progression. The final fit was obtained by varying the parameters in both progressions and by adding the two progressions weighted by their relative intensities.

The calculated and experimental emission spectra are shown in Figure 5. The spectrum was calculated from the parameters given in Table I. All four ring–metal modes are included in the calculation. The calculated spectrum reproduces the pincushion very well. All of the sharp peaks on the cushion are calculated very accurately. The main progression arises from the 333-cm^{-1} Ru–ring stretch mode. The maximum occurs at the 11th quantum of this mode in both progressions I and II.

A magnified portion of the calculated spectrum is compared with the experimental spectrum in Figure 6. The positions and the relative intensities of main peaks in both progressions are accurately calculated. The first sideband of the main peak in the repetitive pattern arises from both the 382- and 400-cm^{-1} modes. These two modes are too close in frequency to be well resolved. The second, weaker sideband arises from the 445-cm^{-1} mode. The position and intensity of this band in both progressions are also correctly calculated.

The overlap (of which the Fourier transform gives the spectrum in Figure 6) versus time shows a clear modulation. For example, the maximum in the first modulation occurs at a time of 0.30 ps, which gives rise to a beat frequency of 112 cm^{-1}.

The calculated spectrum is very sensitive to the displacements of the vibrational modes used in the calculation. For example, when the displacement of the 333-cm^{-1} mode is decreased by 0.2

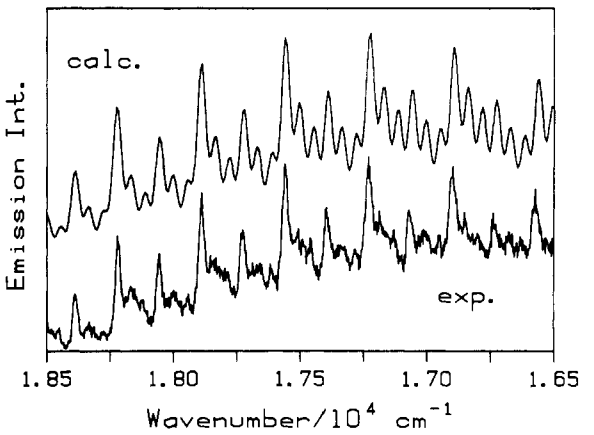

Figure 6. Portion of the calculated and experimental emission spectra of $Ru(Cp)_2$.

(0.008 Å), the intensities of vibronic peaks dramatically change. The intensity of the peak corresponding to the 11th quantum of the 333-cm^{-1} mode decreases by 9%. The intensities of the sidebands decrease by as much as 11%. As another example, when Δ for the 400-cm^{-1} mode is decreased by 0.2, the relative intensity of the main peak (11th quantum of the 333-cm^{-1} mode) vs the most intense sideband increases by 5%. These changes noticeably decrease the quality of the fit in Figures 5 and 6. Because of the sensitivity of the calculated spectrum to small changes in the displacements, the uncertainty in the Δ's is conservatively estimated to be ±0.2.

The appearance of non totally symmetric modes in the emission spectrum has important ramifications to the structure of the excited state. Because they do appear, the point group of the excited state of ruthenocene is lower than that of the structure of the ground state, D_{2h}.[16,18] The point group in the excited state must be one in which these vibrational modes are totally symmetric. The point group that satisfies this condition is C_s. In this symmetry, the 445-cm^{-1} ring–metal stretch and one component of the ring tilt mode are totally symmetric. The involvement of nontotally symmetric modes also contributes to the energy gap between the emission and absorption spectra.[1,19]

The biggest geometry change of ruthenocene in the excited state is along the Ru–Cp bond axis. The Ru–Cp bond length change coming from the totally symmetric Ru–ring stretching mode, Q_1, is 0.12 Å. A previous estimate of bond length change of 0.14 Å based on one totally symmetric Ru–Cp stretching mode is slightly larger because all of the distortions were assumed to be in that one mode.[2] The mass used to convert the dimensionless ΔQ_1 (4.45 or 4.40) into angstrom units is the mass of the Cp ring.[20] Because the normal coordinate Q_1 involves the motion of two Cp rings, the value for the normal coordinate change is multiplied by the factor $1/\sqrt{2}$ to calculate the bond length change of an individual Ru–Cp bond. The change in the asymmetric Ru–ring stretching mode, Q_4, also changes the Ru–Cp bond length. The change is 0.04 Å. The mass used to convert the dimensionless ΔQ_4 (1.20 or 1.05) into angstrom units is the mass of Cp ring. Because the normal coordinate Q_4 involves the motion of two Cp rings, the value for the normal-coordinate change is multiplied by the factor $1/\sqrt{2}$ to calculate the bond length change of an individual Ru–Cp bond. The displacement in Q_1 and Q_4 occurs in the same direction

(17) Bunker, P. R. *Mol. Phys.* **1965**, *9*, 247.

(18) Hargrove, G. L.; Templeton, D. H. *Acta Crystallogr.* **1959**, *12*, 28.

(19) Preston, D. M.; Günter, W.; Lechner, A.; Gliemann, G.; Zink, J. I. *J. Am. Chem. Soc.* **1988**, *110*, 5628.

(20) The formula to convert the dimensionless displacement Δ into Å is

$$\delta = 10^8\left(\frac{6.023 \times 10^{23}}{m}\frac{\hbar}{2\pi c\omega}\right)^{1/2}\Delta$$

where m is the mass involved in the vibration in the units of gram atomic weight (e.g. C = 12 g), ω is the wavenumber of the vibrational mode in cm^{-1}, $\hbar = h/2\pi$ where h is Planck's constant in g cm^2 s^{-1}, c is the speed of light in cm s^{-1}, δ is the displacement in Å, and Δ is the dimensionless displacement.

along one of the Ru–Cp bonds and in opposite directions along the other. Therefore the net bond length change along the Ru–Cp bond is 0.16 Å for one and 0.08 Å for the other.

Summary

The emission spectrum of ruthenocene contains unusually well-resolved vibronic structure. The crystal spectrum consists of two long progressions in the 333-cm^{-1} metal–ring stretching mode, which are separated from each other by 165 cm^{-1}. Each of the peaks of the 333-cm^{-1} progression contains sidebands that are repeated throughout the spectrum. This repetition is explained in terms of beats in the recurrence of overlaps in the time domain. The complete spectrum is accurately calculated by using four displaced normal modes. The major displacement is along the metal–ligand bond axis with minor contributions from ring tilting modes. The point group of the emitting molecule has lower symmetry than that of the molecule in the ground state.

Acknowledgment. This research was made possible by a grant from the National Science Foundation (CHE88-06775). We thank Dr. Lee Tutt and Prof. Mary Henein for preliminary measurements.

Registry No. $Ru(Cp)_2$, 1287-13-4.

Contribution from the Department of Chemistry, University of California, Santa Cruz, California 95064

Assignments of Ground- and Excited-State Spectra from Time-Resolved Absorption and Circular Dichroism Measurements of the ^2E State of (Δ)-$Cr(bpy)_3^{3+}$

Steven J. Milder,† Jon S. Gold,‡ and David S. Kliger*

Received September 9, 1989

Time-resolved absorption and circular dichroism (CD) spectra of the ^2E excited state of (Δ)-$Cr(bpy)_3^{3+}$ are obtained, and assignments of both spectra are made. Excited-state absorption bands at 445 ($\epsilon \simeq 3800$) and 385 nm ($\epsilon \simeq 8000$) are assigned as due to the sum of intensity from both ligand-to-metal charge-transfer (LMCT) and metal-to-ligand charge-transfer (MLCT) transitions. Excited-state CD bands at 430 nm ($\Delta\epsilon \simeq -8$) and 334 nm ($\Delta\epsilon \simeq -11$) are also attributed to a sum of CD intensity from LMCT and MLCT transitions, while an excited-state CD band at 268 nm ($\Delta\epsilon \simeq -26$) is assigned as due solely to an LMCT transition. The magnitudes of the CDs in the ligand long-axis $\pi\pi^*$ transitions are similar for the ^2E excited state and the $^4A_2$ ground state. The excited-state absorption and CD spectra are consistent with a purely metal-centered description of the excited state. Reassignments of the ground-state absorption and CD spectra are made. Both ground- ($^4A_2$) and excited-state (^2E) CD spectra reveal transitions not seen in the unpolarized absorption spectra.

Introduction

The analysis of the circular dichroism (CD) spectra of stable chiral molecular species has long been important in understanding their properties.[1-5] In particular, information about molecular structure, transitions weak in absorption, and the interaction of molecular orbitals can be obtained from CD spectra. In principle, the same analysis of CD spectra is applicable to the CD spectra of transient molecular species, such as chiral intermediates in chemical reactions and the excited states of chiral molecules. However, one is limited, using conventional CD equipment, to looking at intermediates that live for milliseconds or longer. As most molecular excited states do not live this long, the analysis of the CD spectra of excited states obtained by using conventional equipment has been limited to the observation of a few triplet states of chiral organic aromatics.[6-9]

Our laboratory has developed a method for determining the CD spectra of short-lived molecular species, and it has been shown to be useful in obtaining CD spectra with nanosecond time resolution.[10,11] Using this time-resolved circular dichroism (TRCD) method, we have previously reported the CD spectrum of the excited-state absorptions of (Δ)-$Ru(bpy)_3^{2+}$ and (Δ)-$Fe(bpy)_3^{2+}$.[12-14] In these studies, we focused primarily on the magnitudes of the CD of the ligand $\pi\pi^*$ bands, as these magnitudes reflect the nature of the excited states probed.[12-14] For (Δ)-$Ru(bpy)_3^{2+}$, the magnitude of the bpy $\pi\pi^*$ CD decreased and a new, weak CD attributed to the $\pi\pi^*$ band of bpy^- was seen, consistent with the lowest excited state being a single-ligand localized MLCT state. For (Δ)-$Fe(bpy)_3^{2+}$ the magnitude of the $\pi\pi^*$ CD is nearly the same in the ligand field excited state as it is in the ground state and no new $\pi\pi^*$ CD bands were found, consistent with a metal-centered description of the excited state.

In the current work we report the CD spectrum of the excited-state absorption of (Δ)-$Cr(bpy)_3^{3+}$. While the chemistry of the excited state of this complex has been extensively studied,[15-27]

† Present address: Department of Chemistry, Brookhaven National Laboratory, Upton, NY 11973.
‡ Present address: Department of Chemistry, Santa Clara University, Santa Clara, CA 95053.

(1) Kuhn, W. *Annu. Rev. Phys. Chem.* **1958**, *9*, 417.
(2) Schellman, J. A. *Acc. Chem. Res.* **1968**, *1*, 144.
(3) Mason, S. F. *Molecular Optical Activity and the Chiral Discrimination*; Cambridge University Press: Cambridge, U.K., 1982.
(4) Harada, N.; Nakanishi, K. *Circular Dichroism Spectroscopy*; University Science Books: Mill Valley, CA, 1983.
(5) Johnson, W. C., Jr. *Methods Biochem. Anal.* **1984**, *87*, 3226.
(6) Lavalette, D.; Tetreau, C. *J. Phys. Chem.* **1983**, *87*, 1699.
(7) Tetreau, C.; Lavalette, D.; Cabaret, D.; Garaghty, N.; Welvart, Z. *J. Phys. Chem.* **1983**, *87*, 3234.
(8) Tetreau, C.; Lavalette, D.; Balan, A. *J. Phys. Chem.* **1985**, *89*, 1699.
(9) Tetreau, C. *J. Phys. Chem.* **1986**, *90*, 4993.
(10) Lewis, J. W.; Tilton, R. F.; Einterz, C. M.; Milder, S. J.; Kuntz, I. D.; Kliger, D. S. *J. Phys. Chem.* **1985**, *89*, 289.
(11) Kliger, D. S.; Lewis, J. W. *Rev. Chem. Intermed.* **1987**, *8*, 367.
(12) Gold, J. S.; Milder, S. J.; Lewis, J. W.; Kliger, D. S. *J. Am. Chem. Soc.* **1985**, *107*, 8285.
(13) Milder, S. J.; Gold, J. S.; Kliger, D. S. *Chem. Phys. Lett.* **1988**, *144*, 269.
(14) Milder, S. J.; Gold, J. S.; Kliger, D. S. *J. Am. Chem. Soc.* **1986**, *108*, 8285.
(15) Maestri, M.; Bolletta, F.; Moggi, L.; Balzani, V.; Henry, M. S.; Hoffman, M. Z. *J. Am. Chem. Soc.* **1978**, *100*, 2694.
(16) Serpone, N.; Jamieson, M. A.; Henry, M. S.; Hoffman, M. Z.; Bolletta, F.; Maestri, M. *J. Am. Chem. Soc.* **1979**, *101*, 2907.
(17) Rojas, G. E.; Dupuy, C.; Sexton, D. A.; Madge, D. *J. Phys. Chem.* **1986**, *90*, 87.
(18) Rojas, G. E.; Madge, D. *J. Phys. Chem.* **1987**, *91*, 689.
(19) Serpone, N.; Hoffman, M. Z. *J. Phys. Chem.* **1987**, *91*, 1737.
(20) Bolletta, F.; Maestri, M.; Balzani, V. *J. Phys. Chem.* **1976**, *80*, 2499.
(21) Ferraudi, G. J.; Endicott, J. F. *Inorg. Chim. Acta* **1974**, *37*, 219.
(22) Fergusson, J. E.; Herren, F.; Krausz, E. R.; Maeder, M.; Vrbanich, J. *Coord. Chem. Rev.* **1985**, *64*, 21.
(23) Brunschwig, B.; Sutin, N. *J. Am. Chem. Soc.* **1978**, *100*, 7568.
(24) Juris, A.; Manfrin, M. F.; Maestri, M.; Serpone, N. *Inorg. Chem.* **1978**, *17*, 2258.
(25) Gandolfi, M. T.; Maestri, M.; Sandrini, D.; Balzani, V. *Inorg. Chem.* **1983**, *22*, 3435.
(26) Vakac, A.; Zahir, K.; Espenson, J. H. *Inorg. Chem.* **1988**, *27*, 315.

0020-1669/90/1329-2506$02.50/0